EXPERIMENTAL STUDY ON THE CHARGE-EXCHANGE CROSS-SECTIONS OF LOW-ENERGY CARBON IONS IN HELIUM AT GXNU

Guofeng Zhang[1] • Hongtao Shen[1,2]* • Zhenchi Zhao[1] • Junsen Tang[1,2] • Li Wang[1] • Dingxiong Chen[1] • Linjie Qi[1] • Kaiyong Wu[1] • Xinyi Han[1] • He Ouyang[1] • Ning Wang[1,2] • Xiaojun Sun[1,2] • Ming He[3] • Kimikazu Sasa[4] • Shan Jiang[3]

[1]College of Physics and Technology, Guangxi Normal University, Guilin Guangxi 541004, China
[2]Guangxi Key Laboratory of Nuclear Physics and Nuclear Technology, Guilin Guangxi 541004, China
[3]China Institute of Atomic Energy, Beijing 102413, China
[4]University of Tsukuba, Tsukuba, Ibaraki 305-8577, Japan

ABSTRACT. Compared with nitrogen and argon, helium is lighter and can better reduce the beam loss caused by angular scattering during beam transmission. The molecular dissociation cross-section in helium is high and stable at low energies, which makes helium the prevalent stripping gas in low-energy accelerator mass spectrometry (AMS). To study the stripping behavior of ^{14}C ions in helium at low energies, the charge state distributions of carbon ion beams with -1, $+1$, $+2$, $+3$, and $+4$ charge states were measured at energies of 70–220 keV with a compact ^{14}C-AMS at Guangxi Normal University (GXNU). The experimental data were used to analyze the stripping characteristics of C-He in the energy range of 70–220 keV, and new charge state yields and exchange cross-sections in C-He were obtained at energies of 70–220 keV.

KEYWORDS: AMS, charge state yield, cross-section, low energy.

INTRODUCTION

Since the $^{14}N^-$ negative ion is extremely unstable (Bennett et al. 1977), the main interference in radiocarbon-accelerator mass spectrometry (^{14}C-AMS) measurements arises due to the interference of molecular ions such as $^{12}CH_2$ and ^{13}CH, which are not stable at $+3$ charge states and above; as a result, the initial AMS measurements need to be performed at high energies ($>$ MeV) to obtain high charge state carbon ions (C^{3+}, C^{4+}) to exclude the background interference of molecular ions (Purser 1977; Guo 1994). The dissociation of molecular ions $^{12}CH_2$ in charge states 1+ and 2+ was originally reported by Lee et al. (1984). Synal et al. (2000) then found that the intensity of the molecular backgrounds of $^{12}CH_2$ and ^{13}CH in charge states below $+3$ show exponentially decreasing behavior with increasing thickness of the stripping medium, indicating that C^+ and C^{2+} could be used for AMS measurements. Furthermore, Synal et al. (2007) found that when N_2 was used as the stripping medium, the yield of C^+ was high at 200 keV, reducing the energy needed for measurement by the AMS device to approximately 200 keV. At such low energies, however, the angular scattering that occurs during the collision of the ion beam with the stripping medium and the phase space variation in the ion beam at low energies cause a drastic reduction in the transmission efficiency, making it difficult to acquire measurements. Schulze-König (2011) found that C^+ has a higher yield than C^{2+} in helium, where molecular ions such as $^{12}CH_2^+$ and $^{13}CH^+$ have high and constant destruction cross-sections. Moreover, the low atomic number of helium compared to those of other noble gases effectively reduces the efficiency loss due to angular scattering during ion transport; thus, helium is typically used as the stripping gas in low-energy AMS measurements.

*Corresponding author. Email: shenht@gxnu.edu.cn

The earliest study of ion-gas collisions of helium in the keV energy range was performed in 1954 when Stier et al. studied the charge state yields of light ions in H, He, N, Ne, and Ar (Stier et al. 1954). Wittkower and Betz (1973) measured the yield of carbon ions and found that the yield of C^+ at 300 keV is approximately 50% and that the yield increases with decreasing energy (Hveiplund et al. 1972). However, experimental data on the charge state yields and charge-exchange cross-section of C at lower energy range are scarce or not available. To address the lack of data, we investigated C-He interactions in the range of 70–220 keV using the Guangxi Normal University (GXNU) ^{14}C-AMS system.

## GXNU ^{14}C-AMS EXPERIMENTS

GXNU-AMS is the first homemade single-stage AMS in China (Shen et al. 2022). This system was jointly developed by Guangxi Normal University and the China Institute of Atomic Energy. With a maximum design working voltage of 150 kV, a measurement accuracy of 0.6%, and a measurement sensitivity of $^{14}C/^{12}C \approx 2.5 \times 10^{-15}$ (background 50,000 years), GXNU-AMS has a footprint of approximately 2.5 m × 4.6 m and is the only compact and low-energy AMS system developed in China. It includes a cesium sputtering negative-ion source, a pre-accelerator, an injection magnet, an electric quadrupole lens, a main accelerator, a gas stripper, an analysis magnet, an electrostatic analyzer, and a detector, as shown in Figure S1.

To facilitate maintenance on the detector side, the gas stripper, magnetic analyzer, and detector in the GXNU-AMS system are placed at ground potential. The ion source, pre-accelerator, injection magnet, and electric quadrupole lens are mounted on a high-voltage platform, which is insulated from the outside by five ceramic supports at the lower end of the platform. Cs^+ is generated by heating cesium in the ion source to sputter the graphite target and induce C^-. The ion source and injection magnet parameters are adjusted to maintain a stable C^- beam current above 10 µA on the low-energy side. A Faraday cup is used after the injection magnet to measure the $^{12}C^-$ beam current (Figure S1), which is denoted as I_{inject}. Then, the $^{12}C^-$ beam is focused by an electric quadrupole lens and accelerated into the gas stripper through a 150 kV accelerating tube. The gas-stripper tube is 50 cm long and has an inner diameter of 10 mm. A 2-mm inlet aperture in the center of the gas stripper tube is used to supply the external cylinder with helium gas, which is controlled by an S49 32/MT high-precision mass flow meter. A composite molecular pump (JTFB-600F) with a pumping rate of 600 L/s and a mechanical pump set are connected to the lower end of the gas stripper. An ionization gauge (ZJ-27/KF40) placed outside the gas stripper tube is used to record the pressure P at the outer end of the gas stripper tube in real time, which can be used as a proxy for the actual density of the stripping gas in the stripper tube. The gas stripper converts negatively charged ions into neutral and positively charged ions. Then, an analysis magnet with a deflection angle of 90° and a deflection radius of 355 mm is used to select ^{12}C beams with different charge states in a Faraday cup located at the image point of the analysis magnet to determine the intensity of the ^{12}C beams with different charge states, which is denoted as $I_{stripping}$. The different charge states yield F_q, which can be calculated as $I_{inject}/I_{stripping}/q$, where q is the charge state of the ^{12}C ion. Based on the GXNU-AMS facility, the −1, +1, +2, +3, and +4 charge state yields versus the target thickness were measured in the energy range of 70–220 keV.

DATA ANALYSIS

Derivation of the Target Thickness

The charge-exchange reaction between the C ions and the helium inside the gas stripper proceeds as shown in Equation (1) (Zhao 2014):

$$A^m + B^0 \rightarrow A^q + B^n + (n + q - m)e \tag{1}$$
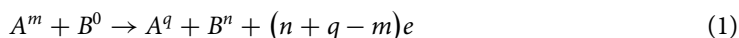
where A is the carbon ion beam stream, B is the target material (helium), and the superscripts m, n, 0, and q represent the charge states of the corresponding ions. In this experimental study, the electron capture and loss occurred during the collision between the C ions and helium. The relationship between the charge state distribution of the C ions and the target thickness was derived from Equation (2) (Datz et al. 1970):

$$\frac{dF_q}{d\alpha} = \sum_{m=-1}^{Z} (F_m \sigma_{mq} - F_q \sigma_{qm}), q = -1, 0, 1, 2 \cdots Z \tag{2}$$

where F is the ratio of an ion beam current with a certain charge state to the original beam current after normalization, α is the target thickness, which is defined as the integral of the gas density along the ion path, σ is the charge-exchange cross-section, and the subscripts m and q represent the charge states of the ions. The flow of stripper gas in a vacuum system can be considered an ideal gas model, and following the equation of state of an ideal gas, the target thickness α can be expressed by Equation (3):

$$\alpha = \rho L = \frac{CPL}{RT} = 7.24 \frac{PL}{T} \tag{3}$$

where ρ is the gas density of helium, P is the average pressure inside the stripper tube, L is the length of the stripper tube, C is a unit conversion factor, R is the gas constant, and T is the thermodynamic temperature. The calculation of the target thickness depends on the acquisition of the absolute pressure P outside the gas stripper tube, as the value of P inside cannot be measured directly with the experimental equipment. According to the semiempirical formula for calculating gas flow in a viscous-molecular flow derived from Knudsen's experiments, $Q = Q_V + bQ_m$, where $b = \frac{1 + \frac{\sqrt{\rho}}{\eta} dP}{1 + 1.24 \frac{\sqrt{\rho}}{\eta} P}$, Q_V is the viscous flow rate, which can be calculated by the Poiseuille formula $Q_V = \frac{\Pi d^4 P}{128 \eta L} (P_1 - P_2)$, Q_m is the molecular flow rate, which can be calculated according to the formula $Q_m = \frac{\sqrt{2}\Pi d^3}{6L\sqrt{\rho}} (P_1 - P_2)$ given by Knudsen (see Umrath 2001 and Loeb 2004). Then, combined with the definition of flow conductivity $C = \frac{Q}{P_1 - P_2}$, the flow conductivity C in the stripper can be deduced as (Seiler 2014):

$$C = \frac{\Pi d^4 P}{128 \eta L} + \frac{1 + \frac{\sqrt{\rho}}{\eta} dP}{1 + 1.24 \frac{\sqrt{\rho}}{\eta} P} \frac{\sqrt{2}\Pi d^3}{6L\sqrt{\rho}} \tag{4}$$

where Π is a constant, d is the aperture of the stripper tube, P is the average pressure inside the gas stripper tube, η is the internal friction coefficient of helium, and L denotes the effective length of the gas stripper tube. The conductance of the external chamber of the stripper tube can then be calculated according to the Knudsen formula. The effective pumping speed of the molecular pump at the exit end of the stripper tube can be obtained based on the gas

continuity equation of the vacuum system, as shown in Equation (5), and then Equation (6) can be derived as follows:

$$Q = P_i S_i = C(P_e - P_j) \tag{5}$$

$$\frac{1}{S_e} = \frac{1}{S_p} + \frac{1}{C} \tag{6}$$

where Q is the gas flow rate, C is the flow conductivity, P_i and S_i are the gas pressure in any section of the pipe and the effective pumping speed of the vacuum pump for that section, respectively, P_e and P_j represent the pressure at different points in the pipe, S_e is the inlet flow rate, and S_p is the effective pumping speed of the vacuum pump. Equations (3)–(6) can then be combined to invert the average pressure P in the gas stripper tube to obtain an accurate target thickness. The relationship among the gas flow meter, the pressure outside the stripper tube and the stripper gas density is shown in Table 1.

Loss Correction of the Ion Beams

During the C-He collision process at low energy, as the thickness of the target in the gas stripper increases, multiple collisions between the C ions and helium occur in the gas stripper, resulting in a more divergent outgoing ion beam. The charge state distribution data that are measured directly at different target thicknesses are not the actual charge state yield distributions. The measurement data are the product of the actual yield of the charge states and a loss function (Maxeiner et al. 2015), as shown in Equation (7):

$$F_{test} = F_{real} \times LOSS \tag{7}$$

$$LOSS = A + B \times \alpha \tag{8}$$

The beam loss caused by the variation in ion phase space and angular scattering can be expressed by the loss function shown in Equation (8) (Maxeiner et al. 2015), where A is the inherent loss due to variation in the ion beam, and B represents the influence factor between the beam loss and the target thickness due to the increase in the target thickness.

Calculation of the Charge-Exchange Cross-Section

The relationship between the different charge state yields and the target thickness can be expressed as a set of first-order linear constant coefficient differential equations (Equation 9). The matrix Σ (Equation 10) contains all the charge-exchange cross-section information. In this experiment, single-electron exchange and double-electron exchange among ions are both considered. The initial incident C^- beam provides the boundary conditions for the system of differential equations, and a large number of data points for the variation in different charge state yields with the target thickness are obtained during the measurement. The experimental data are then fitted by the Runge-Kutta method and the least squares method (Taeara and Russek 1973) to obtain information about the charge-exchange cross-section.

Table 1   The relationship among the MFC, pressure and stripper gas density.

| MFC (mL/min)	Pressure (Pa)	Stripper gas (10^{16} atoms/cm^2)
2.01	5.10E-03	5.11
1.90	4.80E-03	4.81
1.81	4.60E-03	4.61
1.73	4.40E-03	4.41
1.61	4.10E-03	4.11
1.50	3.80E-03	3.81
1.46	3.70E-03	3.71
1.41	3.60E-03	3.61
1.38	3.50E-03	3.51
1.34	3.40E-03	3.41
1.29	3.30E-03	3.31
1.26	3.20E-03	3.20
1.22	3.10E-03	3.10
1.17	3.00E-03	3.00
1.14	2.90E-03	2.90
1.10	2.80E-03	2.80
1.06	2.70E-03	2.70
1.02	2.60E-03	2.60
0.90	2.30E-03	2.30
0.86	2.20E-03	2.20
0.82	2.10E-03	2.10
0.78	2.00E-03	2.00
0.70	1.80E-03	1.80
0.66	1.70E-03	1.70
0.62	1.60E-03	1.60
0.58	1.50E-03	1.50
0.50	1.20E-03	1.20
0.40	9.60E-04	0.96
0.38	9.20E-04	0.92
0.35	8.40E-04	0.84
0.30	7.20E-04	0.72
0.28	6.70E-04	0.67
0.24	5.60E-04	0.56
0.22	5.20E-04	0.52
0.18	4.20E-04	0.42
0.10	2.20E-04	0.22
0.08	1.80E-04	0.18
0.06	1.20E-04	0.12
0.04	7.40E-05	0.07
0.02	2.60E-05	0.03
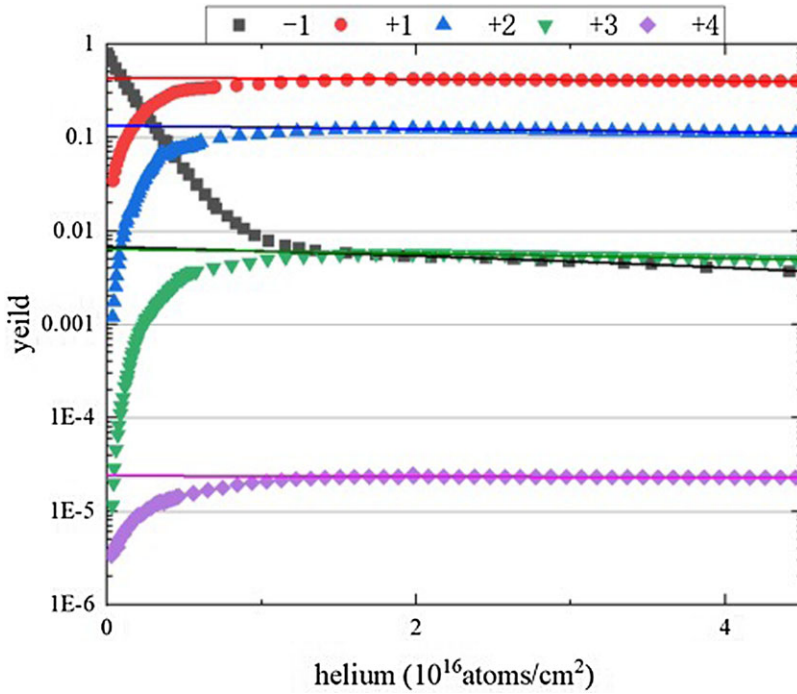
Figure 1   Charge state yield distribution versus target thickness at 190 keV.

$$\frac{d}{d\alpha}\begin{bmatrix} F_{-1} \\ F_0 \\ F_1 \\ F_2 \\ F_3 \\ F_4 \end{bmatrix} = \sum \begin{bmatrix} F_{-1} \\ F_0 \\ F_1 \\ F_2 \\ F_3 \\ F_4 \end{bmatrix} \tag{9}$$

$$\sum = \begin{bmatrix} \sum_{i\in 0,1} -\sigma_{-1,i} & \sigma_{0,-1} & \sigma_{1,-1} & 0 & 0 & 0 \\ \sigma_{-1,0} & \sum_{i\in(-1,1,2)} -\sigma_{0,i} & \sigma_{1,0} & \sigma_{2,0} & 0 & 0 \\ \sigma_{-1,1} & \sigma_{0,1} & \sum_{i\in -1,0,2,3} -\sigma_{1,i} & \sigma_{2,1} & \sigma_{3,1} & 0 \\ 0 & \sigma_{0,2} & \sigma_{1,2} & \sum_{i\in 0,1,3,4} -\sigma_{2,i} & \sigma_{3,2} & \sigma_{4,2} \\ 0 & 0 & \sigma_{1,3} & \sigma_{2,3} & \sum_{i\in 1,2,4} -\sigma_{3,i} & \sigma_{4,3} \\ 0 & 0 & 0 & \sigma_{2,4} & \sigma_{4,3} & \sum_{i\in 2,3} -\sigma_{4,i} \end{bmatrix} \tag{10}$$

RESULTS AND DISCUSSION

Figure 1 shows the behavior of the different charge state yields measured at an ion energy of 190 keV, showing that the yield changes with increasing target thickness. C^- shows an exponential decay with increasing target thickness at low target thickness, while the charge

Table 2   The equilibrium state yields of different ions.

Energy (keV)	+1	+2	+3	+4
70	74.8%	10.4%	0.161%	
100	70.8%	13.1%	0.327%	
130	67.9%	14.4%	0.669%	
160	59.4%	16.9%	0.802%	0.0023%
190	54.3%	14.9%	0.909%	0.0027%
220	50.6%	19.6%	1.23%	0.0041%

states +1, +2, +3, and +4 show increased yields with increasing target thickness, with each positive charge state peaking at a target thickness of approximately 2×10^{16} atoms/cm². The inherent beam loss (factor A in Equation 8) was obtained by measuring the yield of C^- when the gas mass flow is 0 mL/min. The beam losses of different charge states caused by angular scattering were obtained by linear fitting the yield versus the variation in the target thickness after the peak point of the different charge states to determine the influence factor B_i in Equation (8), with i representing the various charge states. The real charge state yield distribution was obtained as $F_{real}=F_{test}/LOSS$. The equilibrium charge state yields obtained after this correction are shown in Table 2, where the C^{4+} beam current was not observed below an energy of 160 keV at the current detector sensitivity. The corrected experimental data of different charge state yields versus the target thickness are shown in Figure 2.

The initial incident C^- showed an exponential decay with increasing target thickness, while the yields of C^+, C^{2+}, C^{3+}, and C^{4+} increased with increasing target thickness and plateaued at a target thickness of approximately 2×10^{16} atoms/cm². The corrected experimental data were then fitted by Equation (9) and Equation (10) to obtain the charge-exchange cross-section values. The relationship between the equilibrium charge state yields and the incident energy is shown in Figure 3. At an incident energy of 220 keV, the C^+ equilibrium state yield after C^--helium collisions was approximately 50%, and this value increased gradually with decreasing energy, with the yield increasing to 75% at an incident energy of 70 keV. On the other hand, the equilibrium charge state yields of C^{2+}, C^{3+}, and C^{4+} tended to decrease with decreasing energy. The measured equilibrium state yields of C^+ and C^{2+} are consistent with those measured previously in similar energy ranges (Figure 4) (Stier et al. 1954; Wittkower et al. 1973; Maxeiner et al. 2015). However, the equilibrium state yields of C^{3+} and C^{4+} are very small, approximately 1.0% and 0.005%, respectively, and thus have little impact on the calculation of the charge-exchange cross-section.

The relationship between the charge-exchange cross-sections and the incident energy is shown in Table 3 and Figure 4. The charge-exchange cross-sections associated with C^+, σ_{01}, and σ_{21} remain high and stable with decreasing energy, while the single-electron exchange cross-sections σ_{10} and σ_{12} show decreasing trends with decreasing energy. Furthermore, the double-electron exchange cross-sections σ_{-11}, σ_{31}, σ_{1-1}, and σ_{13} show similar trends, i.e., σ_{-11} and σ_{31} maintain relatively high and stable values, while σ_{1-1} and σ_{13} show decreasing trends with decreasing energy. Moreover, the values of σ_{01} and σ_{21} (approximately 5×10^{-16} cm²) are much higher than those of σ_{10} and σ_{12} (approximately 5×10^{-17} cm²), and the values of σ_{-11} and σ_{31} (approximately 1×10^{-16} cm²) are much higher than those of σ_{1-1} and σ_{13} (approximately 5×10^{-18} cm²), which explains the increase in the yield of C^+ as the energy decreases. Compared to other studies (see Figure 4), the values of the cross-sections in the same energy
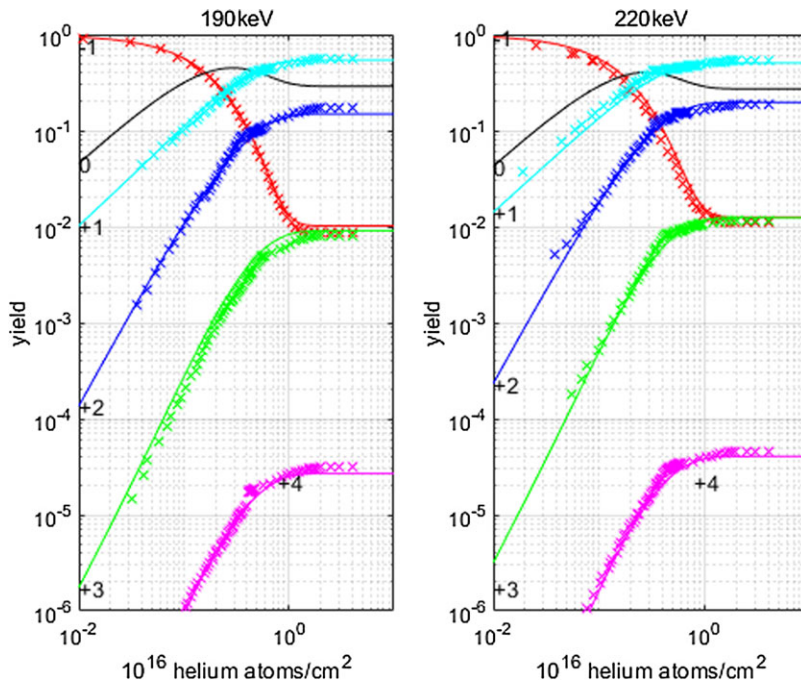
Figure 2 Charge state yield versus target thickness after correction: 90 keV (left), 220 keV (right). The curve represents the fitted data, the symbol × represents experimental data points, and the different colors represent various charge states. Red represents C⁻, black represents a neutral particle (no direct measurement values), light blue represents C+, dark blue represents C2+, green represents C3+, and magenta represents C4+. (Please see online version for color figures.)
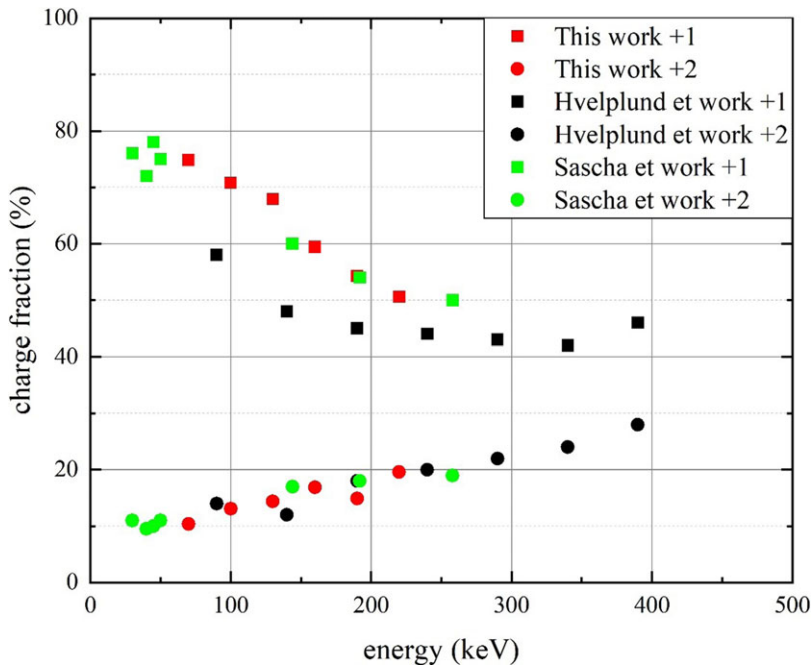

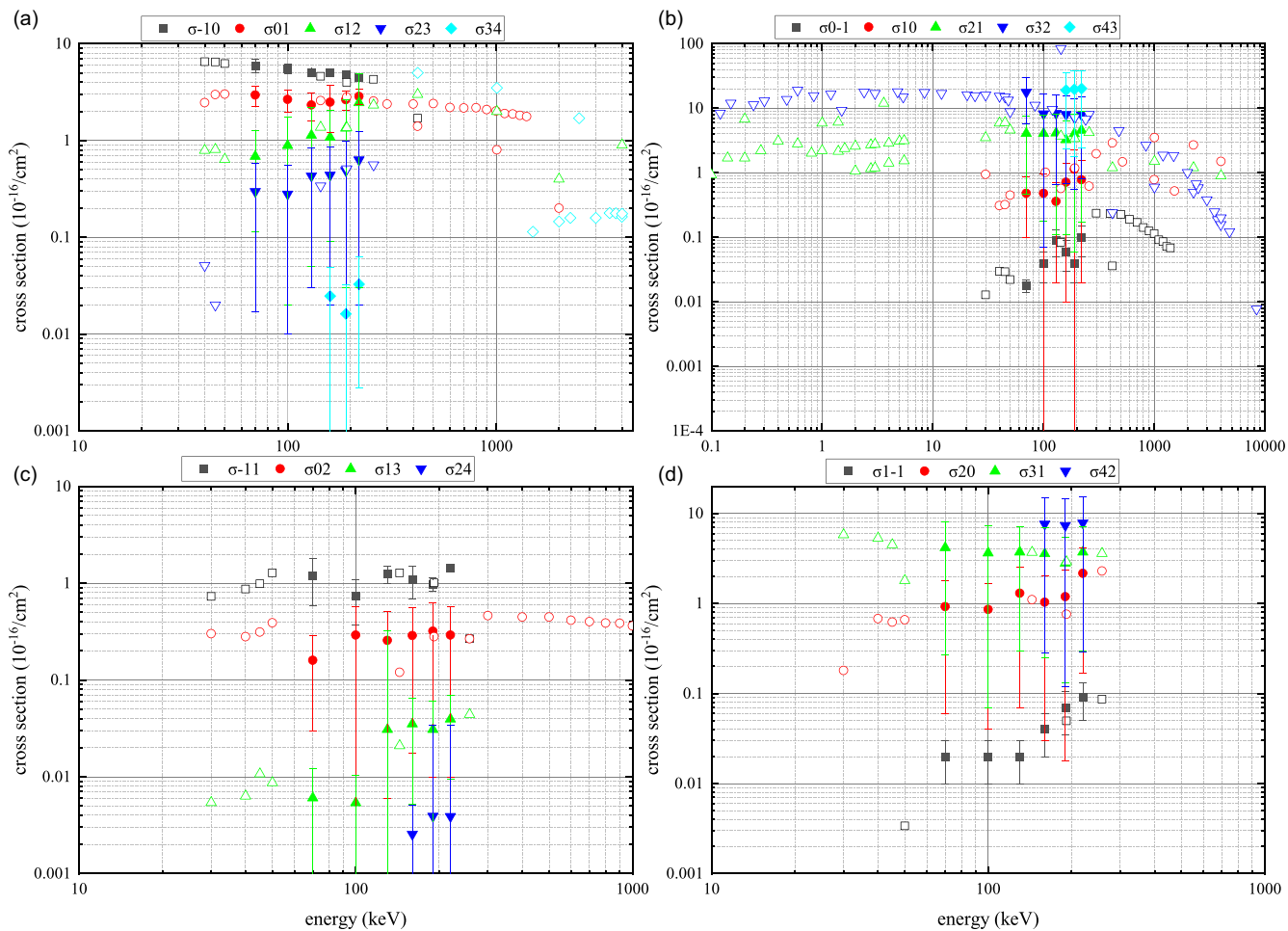Figure 3 Equilibrium charge state yield at different energies.

Figure 4 Charge-exchange cross-sections from the literature (Stier et al. 1954; Wittkower et al. 1973; Maxeiner et al. 2015) (unfilled plot points) and this paper (filled plot points): (a) shows the single-electron loss cross-section, (b) shows the single-electron capture cross-section, (c) shows the double-electron loss cross-section, and (d) shows the double-electron capture cross-section.

Table 3   Charge-exchange cross-sections in the range of 70–220 keV.

$\sigma_{i,j}$	70 keV	100 keV	130 keV	160 keV	190 keV	220 keV
−1, 0	5.94±0.95	5.51±0.61	5.09±0.34	5.05±0.39	4.84±0.15	4.49±0.15
−1, 1	1.18±0.57	0.73±0.37	1.24±0.24	1.09±0.39	0.98±0.15	1.43±0.14
0, −1	0.01±0.008	0.04±0.02	0.09±0.04	0.06±0.03	0.04±0.02	0.10±0.05
0, 1	2.94±0.68	2.56±0.71	2.33±0.74	2.45±1.27	2.64±0.59	2.86±0.53
0, 2	0.16±0.13	0.29±0.29	0.25±0.25	0.28±0.27	0.32±0.31	0.29±0.28
1, −1	0.02±0.01	0.02±0.01	0.02±0.01	0.04±0.02	0.07±0.04	0.09±0.045
1, 0	0.48±0.38	0.48±0.47	0.36±0.34	0.71±0.70	1.13±1.13	0.78±0.76
1, 2	0.69±0.57	0.89±0.85	1.13±1.08	1.08±0.99	1.34±1.31	2.46±2.43
1, 3	0.01±0.006	0.01±0.005	0.03±0.03	0.03±0.03	0.03±0.03	0.04±0.03
2, 0	0.92±0.86	0.86±0.80	1.30±1.23	1.03±1.00	1.18±1.17	2.16±1.99
2, 1	4.08±3.61	4.06±3.80	4.13±4.02	3.25±3.14	4.03±3.97	4.53±4.41
2, 3	0.29±0.28	0.28±0.27	0.43±0.40	0.44±0.42	0.49±0.48	0.63±0.61
2, 4	—	—	—	0.003±0.002	0.004±0.003	0.004±0.003
3, 1	4.17±3.90	3.64±3.57	3.73±3.43	3.58±3.33	2.82±2.67	3.73±3.43
3, 2	17.64±11.88	8.23±8.16	8.31±7.64	8.03±7.35	7.29±6.73	7.81±7.06
3, 4	—	—	—	0.025±0.024	0.016±0.010	0.032±0.030
4, 2	—	—	—	7.63±7.35	7.35±7.23	7.84±7.55
4, 3	—	—	—	19.02±16.66	19.61±17.82	20.10±17.64

range are consistent within the given error (Janev et al. 1988; Nakai et al. 1991; Unterreiter et al. 1991; Rottmann et al. 1992; Ishii et al. 2004; Dmitriev et al. 2010; Santos et al. 2010; Seiler 2014; Maxeiner et al. 2015). The fitting of the double-electron exchange cross-section depends on the calculation of the single-electron exchange cross-section, which introduces a comparably significant error in the measurement.

CONCLUSION

In this experiment, the charge state yield versus target thickness after C- and helium collisions at energies of 70–220 keV was investigated using the GXNU-AMS system, and the experimental charge-exchange cross-section data in the range of 70–144 keV were obtained for the first time. These low-energy charge-exchange cross-section data have great significance in evaluating the charge-exchange process between incident ions and the residual stripping gas in pipelines and their impact on the background of low-energy AMS measurements. The charge-exchange cross section of σ_{i1} shows a steadily increasing trend with decreasing energy, while the cross section of σ_{1i} shows a steadily decreasing trend with decreasing energy. Therefore, the C^+ charge state yield increases from 50.6% at 220 keV to 74.8% at 70 keV, and the increasing charge state yield compensates for the beam loss during low-energy particle transport, thereby enabling more compact AMS systems at energies below 70 keV. The experimental results of this study confirm the experimental findings of Seiler et al. (2014) and the reliability of their proposed AMS theory at low energies below 100 keV, providing attractive (more compact and less expensive) ideas for the design of next-generation AMS systems.

SUPPLEMENTARY MATERIAL

To view supplementary material for this article, please visit https://doi.org/10.1017/S095926952300008X

ACKNOWLEDGMENTS

REFERENCES

Bennett CL, Beukens RP, Clover MR, Gove HE, Liebert RB, Litherland AE, Sondheim WE. 1977. Radiocarbon dating using electrostatic accelerators: negative ions provide the key. Science 198(4316):508–510.

Datz S, Lutz HO, Bridwell LB, Moak CD, Betz HD, Ellsworth LD. 1970. Electron capture and loss cross sections of fast bromine ions in gases. Physical Review A 2(2):430.

Dmitriev IS, Teplova YA, Belkova YA, Novikov NV, Fainberg YA. 2010. Experimental electron loss and capture cross sections in ion–atom collisions. Atomic Data and Nuclear Data Tables 96(1):85–121.

Guo Z. 1994. Modern nuclear analysis techniques and their applications in environmental science. Beijing: Atomic Energy Press. p. 79–127. In Chinese.

Hvelplund P, Lægsgaard E, Pedersen EH. 1972. Equilibrium charge distributions of light ions in helium, measured with a position-sensitive open electron multiplier. Nuclear Instruments and Methods 101(3):497–502.

Ishii K, Itoh A, Okuno K. 2004. Electron-capture cross sections of multiply charged slow ions of carbon, nitrogen, and oxygen in He. Physical Review A 70(4): 042716.

Janev RK, Phaneuf RA, Hunter HT. 1988. Recommmended cross sections for electron capture and ionization in collisions of Cq+ and Oq+ ions with H, He, and H2. Atomic Data and Nuclear Data Tables 40(2):249–281.

Lee HW, Galindo-Uribarri A, Chang KH, et al. 1984. The 12 CH 2 2+ molecule and radiocarbon dating by accelerator mass spectrometry. Nuclear Instruments and Methods in Physics Research B 5(2):208–210.

Loeb LB, Bragg W. 2004. The kinetic theory of gases. 3rd edition. Dover Phoenix Editions. p. 293. ISBN 978-0-486-49572-9

Maxeiner S, Seiler M, Suter M, Synal HA. 2015. Charge state distributions and charge exchange cross sections of carbon in helium at 30–258 keV. Nuclear Instruments and Methods in Physics Research B 361:541–547.

Nakai Y, Sataka M. 1991. Electron capture and loss cross sections in collisions of C atoms with He. Journal of Physics B: Atomic, Molecular and Optical Physics, 24(3):L89.

Purser KH. 1977. US Patent: 4037100, Appl. No: 662968.

Rottmann LM, Bruch R, Neill P, Drexler C, DuBois RD, Toburen LH. 1992. Single-electron capture by 100–1500-keV C+ ions in several atomic and molecular targets. Physical Review A 46(7):3883.

Santos ACF, Sigaud GM, Melo WS, Sant'Anna MM, Montenegro EC. 2010. Absolute cross sections for electron loss, electron capture, and multiple ionization in collisions of C3+ with noble gases. Physical Review A 82(1):012704.

Schulze-König T, Seiler M, Suter M, Wacker L, Synal HA. 2011. The dissociation of 13CH and 12CH2 molecules in He and N2 at beam energies of 80–250 keV and possible implications for radiocarbon mass spectrometry. Nuclear Instruments and Methods in Physics Research B 269(1):34–39.

Seiler M. 2014. Accelerator mass spectrometry for radiocarbon at very low energies [doctoral dissertation]. ETH Zurich.

Shen H, Zhang G, Tang J, Shi S, Wang L, Chen D, Jiang S. 2022. A single-stage accelerator mass spectrometer and its applications at Guangxi Normal University. Nuclear Instruments and Methods in Physics Research B 532:68–72.

Stier PM, Barnett CF, Evans GE. 1954. Charge states of heavy-ion beams passing through gases. Physical Review 96(4):973.

Synal HA, Jacob S, Suter M. 2000. The PSI/ETH small radiocarbon dating system. Nuclear Instruments and Methods in Physics Research B 172(1–4):1–7.

Synal HA, Stocker M, Suter M. 2007. MICADAS: a new compact radiocarbon AMS system. Nuclear Instruments and Methods in Physics Research B 259:7–13.

Tawara H, Russek A. 1973. Charge changing processes in hydrogen beams. Reviews of Modern Physics 45(2):178.

Umrath W. 2001. Fundamentals of vacuum technology. Cologne, Germany: Leybold Vacuum GmbH. p. 14.

Unterreiter E, Schweinzer J, Winter H. 1991. Single electron capture for impact of (0.5–9 keV) C2+ on He, Ar and H2. Journal of Physics B 24(5):1003.

Wittkower AB, Betz HD. 1973. Equilibrium-charge-state distributions of energetic ions (Z> 2) in gaseous and solid media. Atomic Data and Nuclear Data Tables 5(2): 113–166.

Zhao Z. 2014. Experimental study on collision process: noble gas and SF6 with negative ions. Fudan University. In Chinese.